ARTICLE

Self-assembly of supramolecular chemoenzymatic poly-*L*-Phenylalanine [poly(Phe)$_{140}$]

Received 00th January 20xx,
Accepted 00th January 20xx

DOI: 10.1039/x0xx00000x

Alejandra Romero-Montero,[a] Isabel S. Aguirre-Díaz,[a] Jordi Puiggalí,[b,c] Luis J. del Valle[b]*, Miquel Gimeno[a]*

The chemoenzymatic high molecular weight (ca. 20,000 Da) poly-*L*-phenylalanine (ePLP) self-assembly behavior and the nano-morphologies thereof are investigated. Interestingly, this supramolecular ePLP changes from a non-ordered secondary structure when solubilized in water to an α-helix with the addition of only 1vol% HFIP co-solvent, and in relatively low concentration (0.5 mg/mL). The results also indicate a temperature-dependent structure stabilization, wherein the self-assembly process is mainly governed by hydrogen-bonding. The analyses evidence self-assembling under controlled conditions to attain nanotubes with an average diameter of 0.21±0.04 μm, and above 100 μm length. Microbeam synchrotron radiation infrared (SRIR) spectroscopy demonstrates parallel orientations of the amide moieties in the α-helix structure, which is extraordinary for this long chain ePLP. The achievement of this highly homogenous nanotubes is relevant since previous reports only demonstrated this arrangement for end-capped F-moc-containing short oligophenylalanines. In the same way, the conductivity behaviors in the nanotube structure remained unchanged in the range 273-313 K demonstrating its stability by hydrogen bonds, and also, direct dielectric measurements assess a high orientation and stabilization by intra- and intermolecular hydrogen bonds in the nanotubes. These characteristics allow drug delivery assays with tetracycline-loaded nanotubes and further applications are envisaged.

Introduction

The design of new functional, dynamic, and reversible amino acid-based molecular structures and architectures aims to mimic those of natural processes such as the self-assembly of peptides and proteins. These ubiquitous phenomena in natural systems occurs under certain thermodynamic and kinetic conditions in response to specific and local interactions, that causes the formation of ordered structures, with a concomitant entropy reduction in the system as it evolves to one or a few conformers.[1] The construction of peptide blocks has gained interest in the generation of advanced materials in nanobiotechnology and biomedicine owing to their inherent biological origin, structural programmability, biocompatibility and biodegradability, lack of alterations in the immune system, and the use of readily available amino acid precursors.[2-8] Interestingly, the abnormal PP assemblies include nanofibril-type nanostructures, called amyloids, such as the Alzheimer's β-amyloid PP constituted by diphenylalanine (FF) units, which is among the simplest and most common recognition motifs for molecular self-assembly.[9-14] Of note is that the research in these naturally occurring aggregates has developed to the design of artificial peptide nanotubes, commonly bioinspired specifically by the amyloidosis pathological protein aggregation phenomena.[9,10] Conversely, these strategies have also brought novel insights into structural biology and supramolecular chemistry.[11-16]

The polyphenylalanines (PPhe) that self-assemble into discrete and extraordinary geometries are sought to study on several applications, especially in the biomedical field; however, nanotube assemblies are only reported with PPhe oligopeptides with as long as four repeat units having end-capping F-moc from syntheses, which affects the solubility, thereby the control of the self-assembled nanostructure.[17-19] Therefore, a stable and protective groups-free high molecular weight PPhe self-assembly behavior is worth to investigate, and in terms of its physicochemical properties. The peptide under study is enzymatically produced by an innocuous one-step process,[20] which offer several advantages over other chemical or biological approaches,[21] such as the absence of toxicity and side reactions, such as racemization, and water solubility. Worth to note, the reversibility in aqueous media that challenges the consecution of high molecular weights PPs by enzymatic means, as reported elsewhere,[22] has been overcome by conducting the synthesis in neat organic media to attain ca. 20,000 Da average molecular weight.[20] Undoubtedly, an interesting feature of this enzyme-mediated poly-*L*-phenylalanine (ePLP), besides of the absence of end-capping fluorinated adducts from solid state synthesis, and the long peptide chains, is the high water

[a] *Depto. de Alimentos y Biotecnología, Facultad de Química, Universidad Nacional Autónoma de México, 04510 CDMX, México*
[b] *Chemical Engineering Department, Escola d'Enginyeria de Barcelona Est-EEBE, c/Eduard Maristany 10-14, Ed I2, 08019 Barcelona, Spain*
[c] *Institute for Bioengineering of Catalonia (IBEC), The Barcelona Institute of Science and Technology, c/Baldiri Reixac 10-12, 08028 Barcelona, Spain*
† Footnotes relating to the title and/or authors should appear here.
Electronic Supplementary Information (ESI) available: [details of any supplementary information available should be included here]. See DOI: 10.1039/x0xx00000x

solubility in a semi-ordered secondary structure.[19,23] Interestingly, this gives rise to innocuous processability for the self-assembly studies. This work demonstrates that under controlled conditions, the less-ordered aqueous solution of the peptide turns into highly ordered and homogeneous ePLP nanotubes constituted by α-helices. The nanotubes in α-helix structures have parallel orientations of peptide bonds along the axle according to the IR-microbeam synchrotron analyses, which is an extraordinary outcome for such long polyphenylalanine chains. The electrical conductivity and dielectric behavior for these nanotubes have also been investigated, that adds to the envisaged biomedical applications, one of such is their use as drug carrier, which has been ascertained and discussed.

Experimental

Materials

Sigma-Aldrich supplied tetracycline (TC) hydrochloride ($C_{22}H_{24}N_2O_8 \cdot HCl$) and Apollo Scientific Ltd. (Cheshire, UK) supplied 1,1,1,3,3,3-hexafluoro-2-propanol, HFIP [$(CF_3)_2CHOH$]. Sigma-Aldrich supplied *L*-phenylalanine ethyl ester hydrochloride [L-PheOEt•HCl]. Desalting was carried out by the preparation of 11 mL of a potassium hydroxide (39 mmol) solution, to which 22 mL of L-PheOEt•HCl (26 mmol) were added. After stirring for 1 h, the mixture was extracted four times with ethyl acetate (20 mL). The organic extracts were dried over calcium chloride and the solvent removed by rotary evaporation under reduced pressure to give a yellow liquid in a 60% yield. Sigma-Aldrich supplied SC enzyme (Subtilisin Carslberg, Subtilisin A serine S8 endoproteinase EC.3.4.21.62; 27 kDa from *Bacillus licheniformis*). For enzyme activity, SC was incubated in 1,1,1,2-tetrafluoroethane (Norflurane-Dupont by CEI Mexico) in its liquid state (25 bar and 313.15 K) for 3, 6, 24 and 48 h. Then, enzyme was recovered and dissolved (0.064 mg mL^{-1}) in a 10 mM sodium acetate buffer solution with 5 mM calcium acetate (pH 7.5). One unit (U) of protease activity was equivalent to 1 mmol of measured *L*-tyrosine (JT BakerMexico) by the amount of enzyme per minute. Data is the result of three replicates and compared to a control without enzyme. The U for the subtilisin Carlsberg used in this work is 8.39 ± 0.5 mmol/min.mg.

Methods

Enzymatic synthesis of poly-L-phenylalanine ethyl ester

In a typical experiment[20], SC (110 U), L-PheOEt (6 mmol) and a magnetic stirrer were placed in a st-316 cylindrical vessel (40 mL) equipped with two Swagelock (USA) high pressure valves, external ceramic heating jacket connected to a control temperature device, and two thermocouples one measuring the heating jacket and the other inside the reactor vessel. Then, 1,1,1,2-tetrafluoroethane was feed into vessel by an ISCO 160XD Syringe pump (USA). The operational pressure and temperature were 25 bar and 313.15 K, respectively, and the contents were kept under stirring for 24 h. Then, the reactor was depressurized to atmospheric pressure *prior to* open by removing the heating jacket and placed in a 5 °C chamber. Reactor contents were collected in deionized water and centrifuged at 7000 x *g* for 20 min, and the supernatant was recovered and concentrated by ultrafiltration using Amicon ultra 0.5 centrifugal filter for 5000 Da to remove low molecular weight products and reagents. The final sample was stored in an ultra-freezer (REVCO, USA) at -80 °C until use.

Self-Assembly of ePLP

A stock solution (7.6 mg/mL) of ePLP in milli-Q-water was mixed with HFIP as co-solvent to reduce the peptide concentration. Final peptide concentration varied between 7.5 and 0.15 mg/mL, twelve different concentrations were probed to determine the limit necessary to self-assembly. Of each solution were taken 20 □L, deposited over a microscope coverslip into a 24-well plate, and left dry in a cool room at 4 °C for slow solvent evaporation.

Chemical characterizations

FT-IR spectra were acquired in a Perkin-Elmer ATR-FTIR Spectrum 400 instrument. NMR spectra were recorded in a Varian MR-400 spectrometer in DMSO. Synchrotron-based infrared micro-spectroscopy measurements (transmission mode) have been performed at the infrared beamline MIRAS of ALBA synchrotron (Cerdanyola del Valles, Barcelona, Spain) using the Hyperion 3000 microscope coupled to Vertex 70 spectrometer (Bruker, Germany) at 4 cm^{-1} resolution with 256 co-added scans. In this case, the nanotubes were grown directly over infrared transparent windows of CaF_2 (13 mm diameter and 0.5 thickness). All spectra were obtained using a single masking aperture size of 8 × 8 μm. In addition to the intrinsic quasi linear light polarization of synchrotron radiation, the synchrotron light was also polarized at 0 or 90° by a ZnSe holographic wire grid polarizer (Acal BFi Germany GmbH). Raman spectra were acquired using a Renishaw dispersive Raman microscope spectrometer (model InVia Qontor, GmbH, Germany) and Renishaw WiRe software. The spectrometer is equipped with a Leica DM2700 M optical microscope, a thermoelectrically cooled charge-coupled device (CCD) detector (-70 °C, 1024 × 256 pixels) and a spectrograph scattered light with 2400 lines mm^{-1} of grating. The experiments were performed at a 532 nm excitation wavelength and with a nominal laser power between 1 and 100 mW output power. The exposure time was 10 s, the laser power was adjusted to 1% of its nominal output power and each spectrum was collected with three accumulations. Raman spectra were collected in a spectral range from 600 to 1600 cm^{-1} with the same measurement parameters. Circular dichroism (CD) spectra at the far-UV region were recorded with a Chirascan-plus *q*CD spectrometer (Applied Photophysics, APL; UK) equipped with a temperature-controlled cell, using a path length 10 mm. Electrophoresis polyacrylamide gel was prepared at 15% resolving and 4% stacking. Sample was diluted to 15 mg/mL of ePLP. The sample was diluted 1:4 with sample buffer (SDS reducing buffer), and heated at 95 °C for 10 min. Reference bands of BSA and Lyz solutions were loaded using the same tracking dye. All samples were exposed to an electric field of 120 V for 2 h. After that time, the gel was dyed using a Coomassie blue/methanol/acetic acid (0.1%:40%:10%) solution and,

subsequently, washed-out with an aqueous solution of 40% of methanol and 10% of acetic acid.

Nanotubes Morphology.

Optical microscopy images were collected using a Zeiss Axioskop 40 Pol light polarizing microscope (Carl Zeiss, Göttingen, Germany) where nanotubes samples were grown on a glass coverslip. Scanning electron microscopy (SEM) was carried out using a Focused Ion Beam Zeiss Neon40 scanning electron microscope operating at 5 KV. Nanotube samples were grown on a glass coverslip and deposited on pin stubs of aluminum, and sputter-coated with a thin layer of carbon. Atomic force microscopy (AFM) images were acquired in a Molecular Imaging PicoSPM and a NanoScope IV controller, under ambient conditions. AFM tapping was operated at constant deflection with 1 Hz row scanning frequency. Measurements were performed on various parts of the morphologies, which produced reproducible images similar to those displayed in this work. Scan window sizes ranged from 5 × 5 μm^2 to 80 × 80 μm^2.

Conductivity Measurements

For a first screening, proton conductivity measurements were performed with a dry self-assembly membrane. The conductivity was determined by means of impedance measurements using AutoLab PGSTAT302N frequency response analyzer (FRA) at AC amplitude of 10 mV. The frequency interval employed for the measurements ranged from 10kHz to 10mHz. The self-assembly samples were grown on a two stainless steel disks (blocking electrodes composed by AISI 304 type). 200 µL of a solution with a peptide concentration of 0.76 mg/µL in water/HIFP (94:6) were deposited and left dry at 4 °C. Then, samples were sandwiched within the disks, separated by a Teflon holder, corresponding to the through-plane conductivity homemade cell configuration. The cell used was completely described previously.[24] Finally, for the assay the dry self-assembly samples thickness values were measured with a Neurtek Mega-Check pocket FE device. The high-frequency data of the Nyquist plot corresponds to the combination of bulk resistance (R_b) and capacitance of the polymeric membrane-electrode system and the fitting of experimental results with electrical equivalent circuit. Proton conductivity of the samples was calculated using the following:

$$\sigma = \frac{L}{R_b A}$$

Where σ is the proton conductivity (S cm^{-1}), L the thickness (cm) of the polymer membrane, A is the contact area between the electrodes and the polymer membrane (i.e., the electrode surface area, 1.766 cm^2), and R_b the bulk membrane resistance (Ω) calculated from the Nyquist plot.

Dielectric measurements

Proton conductivity measurements were performed with dry nanotubes grown on the steel electrode surface. The reported conductivity values correspond to the average of measurements performed with two samples at room temperature. Compression pressure was fixed at the minimal distance allowed by the screws used to seal the cell. A Novocontrol Alpha analyzer was used for broadband dielectric spectroscopy (BDS) measurements. The sample was placed in a stainless steel parallel-plate capacitor specially designed for the analysis of liquid samples, with the two electrodes kept at a fixed distance by means of silica spacers of 50 µm diameter. Temperature control of the capacitor and thus of the sample was achieved with a nitrogen-gas flow cryostat with an error not higher than 0.1 K. The e-PLP nanotubes samples were heated to 298 K prior to measurement to eliminate any remaining solvent. The sample was then rapidly cooled to 133 K and isothermal spectra were then acquired by increasing the temperature in a stepwise fashion, waiting each time 5 minutes for temperature stabilization. Spectra were acquired in the frequency (v) range and temperature between 10^{-2} and 10^7 Hz, and 273-493 K, respectively.

TC loading into the e-PLP nanotubes and release experiments

A stock ultrafiltered solution (7.6 mg/mL) of ePLP in milli-Q-water was mixed with HFIP as co-solvent to reduce the peptide concentration to 4.2 mg/mL. This solution was mixed with a 25 mg/mL of TC aqueous solution to final mass proportions of 1:1, 1:0.5 and 1:0.33 ePLP/TC. Then, 20 µL of each solution was deposited on a microscope coverslip and left dry in a cool room to grow the self-assembly. TC-loaded and unloaded (controls) nanotubes grow on a microscope coverslip were placed into Falcon tubes. Phosphate buffered saline (PBS) solution of pH 7.4 with 20 % v/v of ethanol was considered as the release medium. Assays, which were performed in triplicate, were carried out by immersing sample nanotubes in 20 mL of the release medium and using a rotating agitator (80 rpm and 37 °C). The medium (1 mL) was removed at predetermined time intervals and replaced by fresh one. The removed medium was used to quantify the released TC by measuring its absorbance in a UV-vis-NIR Shimadzu 3600 spectrophotometer. Finally, the nanotubes were dissolved in water and the residual TC-loaded in ePLP was quantify by UV-vis. Calibration curves for TC (y = 0.0039x + 0.037; R^2=0.9997) and ePLP (y = 1.0337x + 0.0276; R^2=0.9994) were obtained by plotting the absorbance against concentration from triplicate samples. Samples before and after the drug release were analyzed using a confocal laser scanning microscope (LSM 900 Zeiss). Images were taken with a camera controlled by ZEN 2.6 blue edition software (Carl-Zeiss Microscopy GmbH, Jena, Germany). The Higuchi and first-order models were applied to analyze the drug release:

$$\frac{M_t}{M_0} = k_H t^{1/2} \qquad \left(0 \le \frac{M_t}{M_0} \le 0.6\right) \qquad \text{(Higuchi model)}$$

$$\ln\left(1 - \frac{M_t}{M_0}\right) = a - k_1 t \quad \left(0.4 \le \frac{M_t}{M_0} \le 1.0\right) \qquad \text{(First-order model)}$$

where k_H and k_1 are the Higuchi and first-order release constant, respectively; a take into account the release in the first step, M_t is the percentage of drug released at time t, and M_0 is the drug equilibrium percentage (considered as the maximum drug percentage).

RESULTS AND DISCUSSION

The H^1 NMR (supplementary data Figure S1) and SDS-PAGE electrophoresis (supplementary data Figure S2) corroborates molecular weight for ePLP after the ultrafiltration process (ca. 20,000 Da). The recorded UV-vis spectra varying the amounts of ePLP plotted against product concentration shows the characteristics bands of the absorption maxima at 251, 257 and 263 nm, which are assigned to the π-system of the aromatic groups in the repeat units (see UV absorption spectra for several ePLP concentrations and calibration curve in supplementary data Figures S3). The CD spectra recorded in water (0.5 mg/mL) and in urea (1 M) provide information about the structure and the role of the hydrogen-bonding in the organization of ePLP in the initial assembly process, as shown in Figure 1. Of note is that the water-assisted hydrogen bonds are key in self-assembly arrangement for protein fibril formation, which occurs in the amyloid proteins involved in the development of degenerative diseases. Therefore, the hydrogen bonding sites are driving forces towards the organization, formation, stabilization of the secondary structure, and for the folding of the peptide.

The bands in the spectra display a mixture of random, β-sheet and α-helix structures in 31.29, 52.93 and 15.78 %, respectively, as calculated by Dichroweb.[25,26] The spectra recorded in neat water at different temperatures displays a broad and positive CD signal, which decreases with the increase in the temperature. This behavior can be intuitively understood by the corresponding UV absorptions (supplementary data Figure S4).[27] The carbonyl transition (n→π*) at 222 nm displays a constant decrease during the heating cycle, which is related to the loss of structural integrity for this moiety, which in turn, disrupts the hydrogen bonding between the amine and carbonyl oxygen atom.[28] Therefore, these evidence that the temperature influences the stabilization of the hydrogen bonds in the ePLP.

On the other hand, when the CD is conducted with urea (Figure 1b), which restricts water interpenetration and triggers the unfolding and denaturation of peptides.[29] the intensity and the intensity-gradient of the band at 222 nm are smaller and thinner than that in water (see insets in Figure 1).

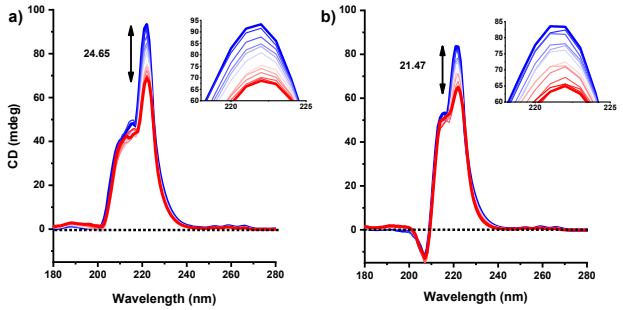

Figure 1. CD spectra upon heating from 25 °C (blue) to 90 °C (red) for water-solubilized (a), and urea-solubilized (b) ePLP.

Undoubtedly, this behavior is tied to the unfolding process caused by the urea on the ePLP, which is also corroborated by an exciton couplet (205-210 nm) owing to the interaction between the carbonyl group and the aromatic residue.

In conclusion, the results suggest that the structure stabilization dependents on temperature in a process mainly governed by hydrogen-bonding.

Assembly of the ePLP into nanotubes

The sweep of thermodynamic conditions of concentration (0.15-0.5 mg/mL), and HFIP co-solvent demonstrate that the homopeptide self-assembles in several geometries at 4 °C, as shown in the representative optical micrographies in Figure 2.

Interestingly, the concentration of 0.5 mg/mL allows a self-assembly into nanotubes with homogeneous morphology, which is best with 1 vol% of HFIP. The optical micrographs evidence that length and their presence increase with the increase in water in the mixture, as shown in Figure 3.

The SEM and AFM analyses also corroborate that ePLP self-assembles best with a 1:99 HFIP/H_2O ratio in well-defined nanotube morphology. The average diameter of these tubes by AFM is 0.21±0.04 μm, whereas the length is established in several hundreds of microns (Figure 4). It is remarkable that under these conditions the self-assembly process attains homogenous average sizes, whereas there is poor control of the morphologies with other experimental conditions.

It is worth to note that previously reported nanotubes from dimers and oligomers of PPhe required higher PPhe concentrations and co-solvent contents than this work to attain homogenous nanotubes.[30-32] Additionally, the tubes obtained with this enzyme-mediated peptide have smaller diameters than those reported for oligophenylalanines.[18,33-35]

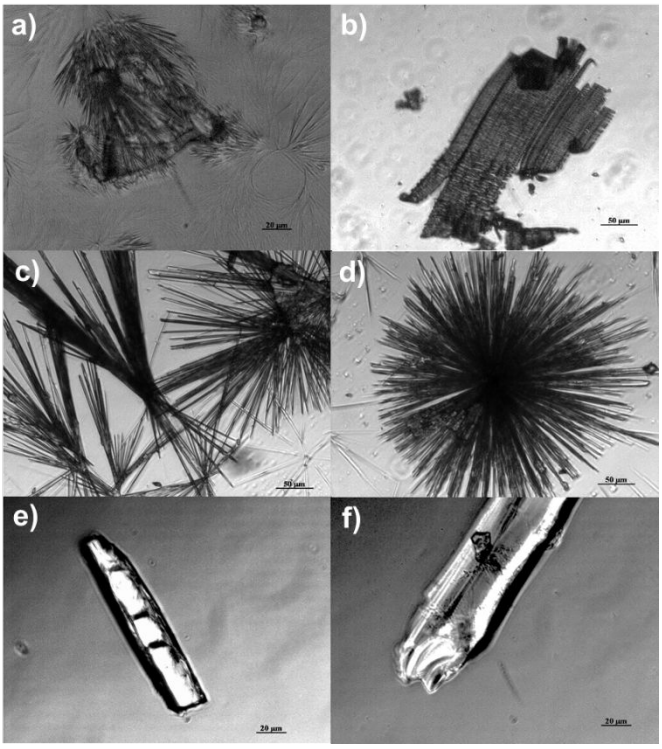

Figure 2. Optical micrographs of self-assemble of ePLP obtained at 4 °C in a concentration of 0.15 $mgmL^{-1}$ in HFIP/H_2O 9:1 (a,b); 0.375 $mgmL^{-1}$ in HFIP:H_2O 6:94 (c,d); and ePLP 0.075 $mgmL^{-1}$ in 1:9 (e) and 2:8 of HFIP:H_2O (f).

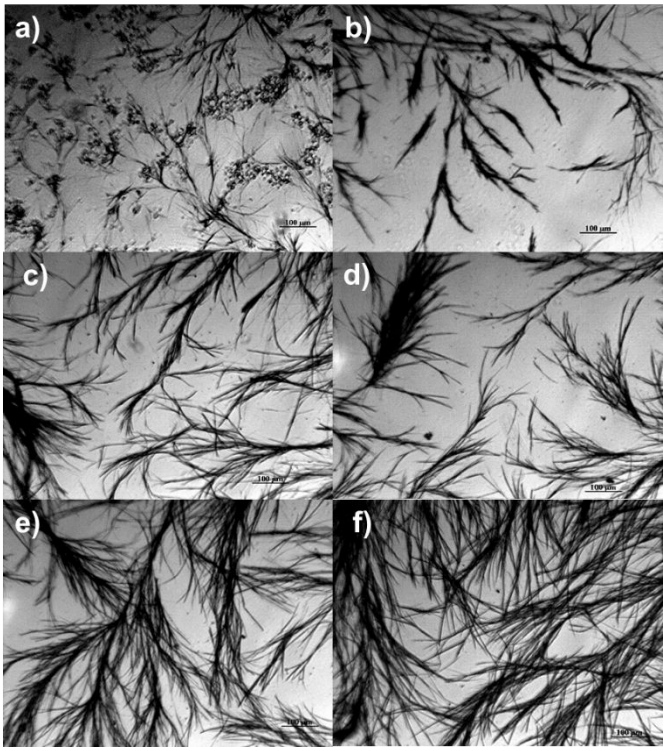

Figure 3. Optical micrographs of self-assembled ePLP (0.5 mg·mL^{-1}) at 4 °C in HFIP/H_2O 2:3 (a), 1:4 (b), 1:9 (c), 6:94 (d), 2:98 (e), 1:99 (f).

The experimental evidence indicate that the control of the nanotube formation is related to the increase of water in the mixture while keeping low molecule concentration and low co-solvent content.

Of note is the relatively high ordering in neat water, which is an outstanding result for further biological studies. The non-covalent interactions in water are specific and they allow unique modes of supramolecular assemblies, thereby the aqueous supramolecular polymers offer the possibility of creating biocompatible systems with great potential in medical applications.[36]

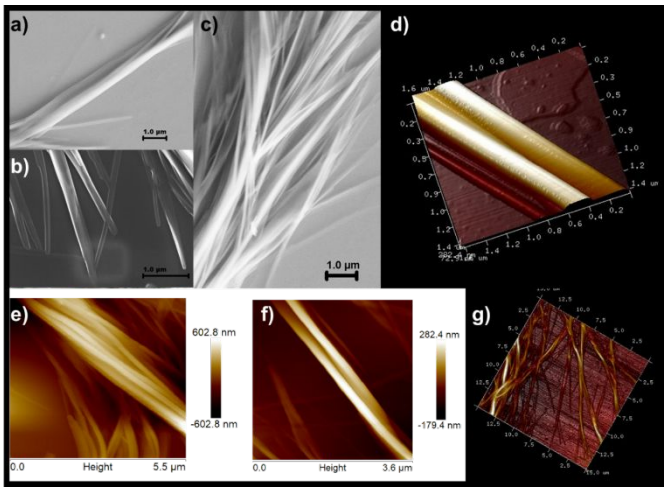

Figure 4. Micrograph images for the ePLP nanotubes obtained at 4 °C and 0.5 mgmL^{-1} in 1:99 HFIP/H_2O; SEM (a-c) and AFM (d-g).

FTIR and SR-IR analyses

Figure 5-a shows the FTIR spectra for a nanotube sample with 0.5 mg/mL (red) peptide concentration, and that for the non-assembled ePLP (blue). The NH stretching vibration gives rise to the band at 3,530 cm^{-1} assigned to amide A, which frequency depends on the strength of the hydrogen bond and correlates to the Fermi resonance doublet with the second component (amide B) at 3,115 cm^{-1}. Noteworthy, the amide I band (1,600-1,700 cm^{-1}) changes when the ePLP is self-assembled, because this is sensitive to the effects of the existing hydrogen bonds.

The deconvolution for this amide I (Fig 5-b below) suggests that the ePLP shifts from a mixture of β-sheet (1,638 and 1,565 cm^{-1}), random structures (1,608 cm^{-1}) and α-helix (1,583 cm^{-1}) to adopt an α-helix with 1% HFIP (Fig 5-b above), which agrees with the CD spectra. The specular SR-IR using synchrotron radiation demonstrates that the formation of nanotubes is likely triggered by the long-range orientation of peptide bonds along the axis, creating a hydrophilic region inside the helix with outside-oriented hydrophobic aromatic rings. This agrees with the documented self-assemblies for diphenylalanine and F-Moc end-capped tetraphenylalanine.[18,37-39] Therefore, the synchrotron analysis demonstrates that the ePLP behaves as the previously reported phenylalanine oligomers. These supramolecular assemblies are built *via* hydrogen-bonding among neighboring amino acids, which constitute strong supramolecular interactions which deeply stabilize secondary structures in peptides and proteins.

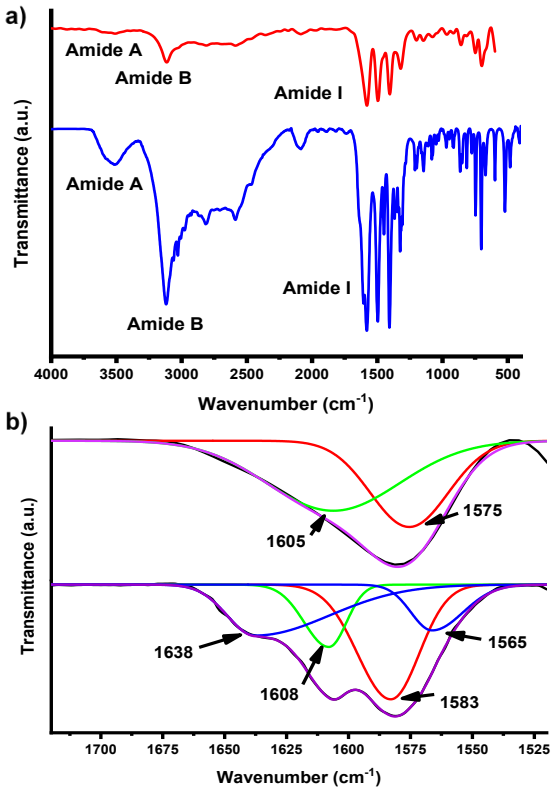

Figure 5. (a) FTIR spectrum for self-assembled (above) and lyophilized ePLP (below) with labeling of main bands. (b) Fourier deconvolution in amide I region for FTIR spectra, non-assembled (above spectrum); and self-assembled (below spectrum).

This constitutes a relevant discovery because the formation of such materials is starting to pave the way for emergent applications such as the development of biomimetic membranes with inner channels for small molecules transport, among them, novel controlled drug delivery systems[40,41] in which the responses are enhanced by long-chain PPs.

In the SRIR study for the nanotubes, shown in Figure 6-b, the samples are grown directly over the CaF_2 infrared transparent windows onto a group of nanotubes horizontally oriented, as shown in the optical micrograph in Figure 6-a. The areas with horizontally oriented tubes have evidently opposite absorption to the vertically oriented (horizontal disposition for a 0° polarized spectrum). This demonstrates that the C=O bond of amide moieties are mainly oriented parallel to the helical axis.

The disappearance of this band in the spectrum acquired with 90° polarization upholds a long-range parallel orientation for amide moieties. A graphical representation of the achieved high molecular weight ePLP self-assembly is depicted in Figure 7.

This remarkable feature is strongly indicative for the formation of hydrophilic inner pockets inside these nanotubes according to a highly directional hydrogen bonding of neighboring amino acids.

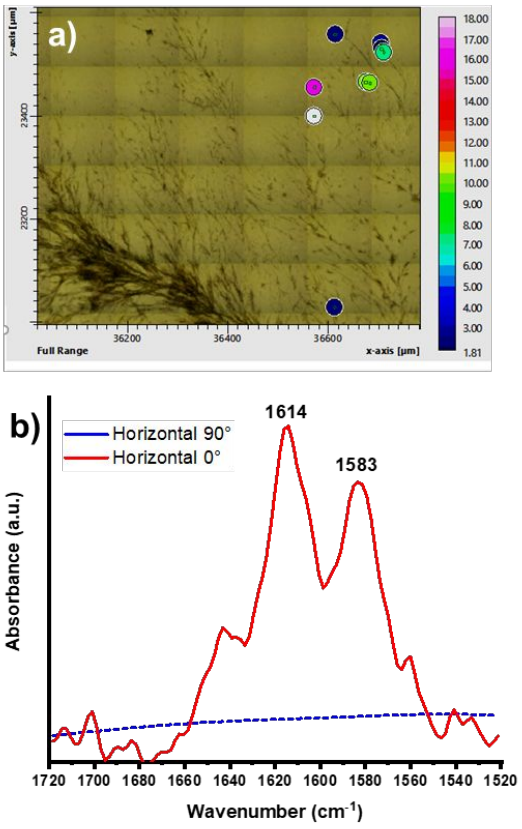

Figure 6. Optical micrograph displaying horizontally and vertically oriented ePLP nanotubes selected for measurements (points) (a); and polarized SRIR spectra of ePLP tubes with horizontal and vertical orientations, acquired with 0 and 90° polarizations (only for the horizontal orientation) (b).

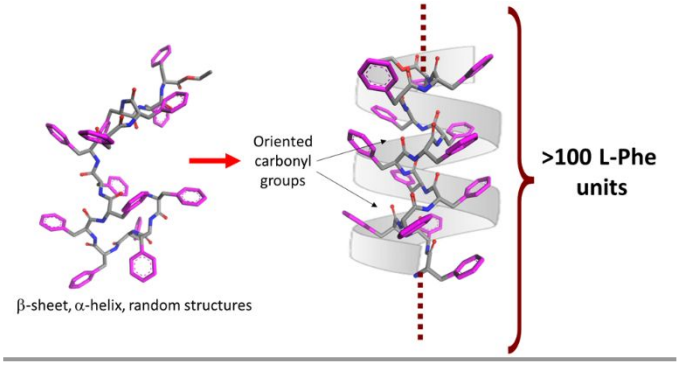

Figure 7. Schematic representation of ePLP assembly

Conductivity measurement in the ePLP nanotubes

The Nyquist (Supplementary Figure S5) graphical representation shows a smaller resistance for the ePLP nanotubes sample than that of the low-ordered ePLP. The fitted equivalent circuit (Supplementary Figure S6) displays good correlation, and statistically lower than 10%.

The calculated proton conductivity and the thickness of the samples are shown in Table 1.

There are few studies on conductive PPs, although the existence of conductive oligopeptides is recognized, this are not formed by purely amino acid units but functionalized with molecules such as thiol.[42] Interestingly, the directional proton-transfer dependence is correlated with the electric field generated by the net molecular dipole, which is also known to be present in α-helical oligopeptides. In the same way homopeptides of up to twenty units of alanine, lysine, glutamic acid, and tryptophan are reported to display a dependence of conductivity with the secondary structure.[42,43]

Other studies demonstrate that the proton conduction capacity of amyloid-like fibers increase with the number of fibers crossing at the same point.[44] Furthermore, Yardeni et al. reports that in dehydrated conditions, the long-range ordering induced by the aromatic side chains play a key role, which is evident from higher proton conduction through peptide nanotubes containing naphthyl- capped lysine units.[45]

In summary, the simple and intrinsic ability to self-assembly into ordered α-helix nanotubes for this ePLP emerges as a promising feature for further biotechnological applications. Extensive studies have revealed that semiconductivity is an inherent property for some peptide-based nanostructures, exhibiting notable characteristics that allows the development of bioinspired entities into novel functional materials.[46]

Table 1. Sample structure of polymer, resistance (R), proton conductivity (⍰) and sample thickness (ST)

Sample structure	R_b^*(Ω)	σ^* (S cm^{-1})	ST** (µm)
ePLP (disordered/bulk)	5.8×10^3	6.2×10^{-7}	25±3
ePLP (nanotubes)	1.8×10^2	3.2×10^{-6}	4±2

*Measured in dry state at room temperature, fitting the impedance data obtained to the equivalent circuit shown in Figure S5. ** Sample thickness (ST) was measured with a Neurtek Mega-Check pocket FE device.

Dielectric behavior of the ePLP nanotubes

To scale the intermolecular electrostatic interactions in our ePLP, which generally, varies according to the size and composition of each polypeptide chain, an accurate determination of the dielectric constant is essential. Direct measurements of dielectric constants of dry proteins span a range from 2.5 to 3.5. These values are determined by measuring the capacity of crystalline samples, which agree with chemical shift perturbation measurements. However, in addition to amino acids, proteins in practice contain solvent molecules as well as organic and inorganic cofactors. These affect their dielectric constants, and, in most cases, the effective dielectric constant is significantly different from the measured values for dry proteins.

In this regard, Figures 8a and 8b show the evolution of the real part (ε') of the dielectric constant of the disordered (powder/bulk) ePLP sample and that consisting of self-assembled ePLP nanotubes, respectively. This physical property was measured in the frequency from 10^{-2} to 10^{7} Hz range, and at different temperatures (273-493 K). Noteworthy, this allows to assess a variety of biochemical interactions such as electron and proton transfer, voltage gating, ion channel selectivity, charge separation, and protein-protein and protein-ligand interactions, which are ruled in a large extend by the electrostatic-potential surface. From Figures 8a and 8b can be inferred that the dielectric constant (ε') increases as a function of the temperature and decreases from the lowest frequency upwards.

This is particularly demonstrated in Figures 8c and 8d where this variation is more evident at low frequency (e.g., 10^{-2} Hz) compared to that observed at moderate / high frequency (e.g., 10^{3} Hz). Thus, at 10^{-2} Hz the dielectric constant of the non-ordered sample shows a rapid increase (from a value of 1.5) with the temperature and this can possibly be explained by the reorientation of the dipole of ePLP molecules. However, in the ePLP nanotube, the dielectric constant with a value of 1.7 remains in the 273 K-313 K temperature range (as shown in the gray area of Figure 8d). This resistance of the dielectric constant to change must be a consequence of the self-assembled structure of the nanotubes. In other words, the dipoles are already oriented and stabilized by the formation of intra- and intermolecular hydrogen bonds. This hypothesis can be sustained because at temperatures higher than 323 K the destabilization of the hydrogen bonds begins to occur in the nanotubes.

On the other hand, the non-variation of the dielectric constant at 10^{3} Hz even at temperatures greater than 400 K, with values of 1.5-1.7 for the low-ordered sample and 2.1-2.2 for the nanotubes, allow us inferring that they are free of water molecules that could interfere with the dielectric constant. Noteworthy, the sample with ePLP nanotubes accumulate greater charge than the low-ordered one, as can be deduced by the slope of the ε' vs T curve at low frequency (Figure 8d). The maximum temperature is 493 K (i.e., the melting temperature according DSC data (Supplementary Figure S7).

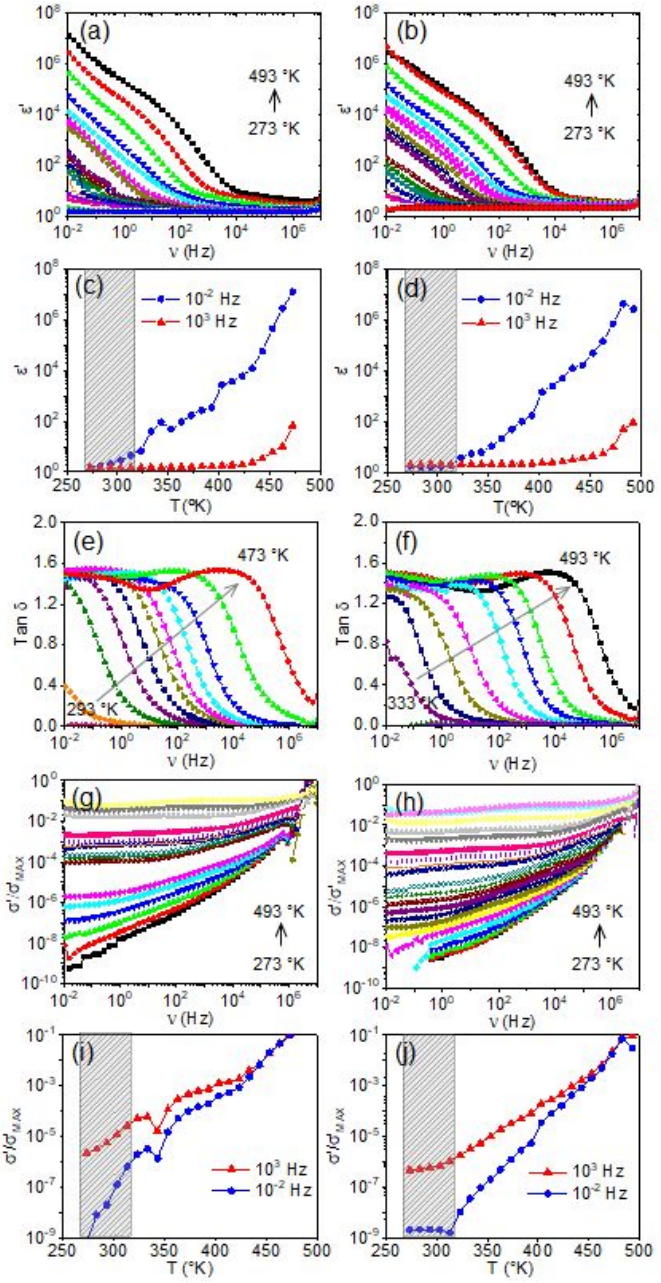

Figure 8. Dielectric behavior of non-ordered ePLP (a, c, e, g and i) and nanotubes (b, d, f, h and j) samples. Dielectric constant (a, b), plot of dielectric constant vs temperature (c, d), dielectric loss vs frequency (e, f), electrical conductivity vs frequency (g, h) and conductivity vs temperature (i, j).

Contrarily, the variation of the imaginary part is linear for these ePLP samples (Supplementary Figure S8). According to the general theory of dielectrics, if a pure substance has only one type of polar molecule, the dielectric dispersion curve is expected to fall from one plateau to another as field frequency is increased. In this way, the melted sample has totally lost its dielectric properties. The loss factor or dielectric loss (tan δ) is calculated from the ε''/ε' ratio, and the dielectric loss against the frequency plotted for different temperatures is shown in the Figures 8e and 8f. A single *α*-dispersion is detected for both samples, and a dependence of dielectric loss with temperature

was noticeable. In the ePLP sample containing nanotubes, this *α*-dispersion begins at higher temperatures (e.g., 333 K) and it extends regularly until the maximum loss at 493 K, while the loss starts at 293 K for the less-ordered sample, with a maximum at 473 K. These results demonstrate that the organization of the ePLP in nanotubes confers greater resistance to dielectric losses. It is known than α-dispersion, which remains the least understood, is generally attributed to either relaxation of counterions surrounding the charged biomolecules or migration of ions through voids in membranous materials. In the case of the organization in nanotubes, the transit of the ions could be directed through the interior of their channel, thus avoiding dielectric losses.

The real part of the DC electrical conductivity (σ) is shown in Figures 8g and 8h for the two ePLP samples, respectively. A semiconductor behaviour is inferred in both cases, but significant differences are detected in the distribution of their values as a function of both frequency and temperature. This static conductivity measures the dynamic changes in the dielectric constant and Figures 8i and 8j data establish that the conductivity of the two studied ePLP samples could be distinguished by a temperature dependence. Therefore, at low and moderate frequency, the non-ordered ePLP sample showed a temperature dependence following several stages (Figure 8i). However, for the nanotubes, a linear dependence is observed at temperatures higher than 323 K, whereas, at lower temperatures (e.g., 273 K- 313 K), the nanotubes display constant conductivities of 10^{-8} S/cm and 10^{-6} S/cm at low and moderate frequencies, respectively. These latter results are not surprising since no changes occur in the dielectric constant and consequently neither in its conductivity. The nanotube arrangement of ePLP controls proton transport, and the orderly stacking of phenylalanine rings could handle the electronic motion.

TC loading in the enzyme-mediated PLP nanotubes

The physicochemical characterization of the amphiphilic ePLP nanotubes indicates their potential for many applications including drug delivery. For the latter, TC is an excellent explorative molecule for in-vitro studies owing to its fluorescence and broad-spectrum antibiotic characteristics. The nanotube formation from the 1:99 ratio (HFIP:H_2O; 0.5 mg/mL; 4 °C) proceeds accurately with the presence of the drug in 1:1, 1:0.5 and 1:0.33 (wt:wt; ePLP:TC) ratios.

The presence of the TC is readily verified by confocal microscopy (Figure 9). Control sample micrograph in Figure 10a shows initial auto fluorescence from the peptide, notwithstanding a qualitative increase with the TC loading (Figure 9 b-e). The TC fluorescence inside the nanotubes is evidenced, although TC adsorption on the surface cannot be ruled out, owing to electrostatic interactions and hydrogen bonding. The latter is corroborated by Raman spectroscopy (See supplementary data S9 for Raman spectra), which indicates that the hydrogen-bonding interactions exist between outer PLP layers and TC, thus altering the local chemical environment.

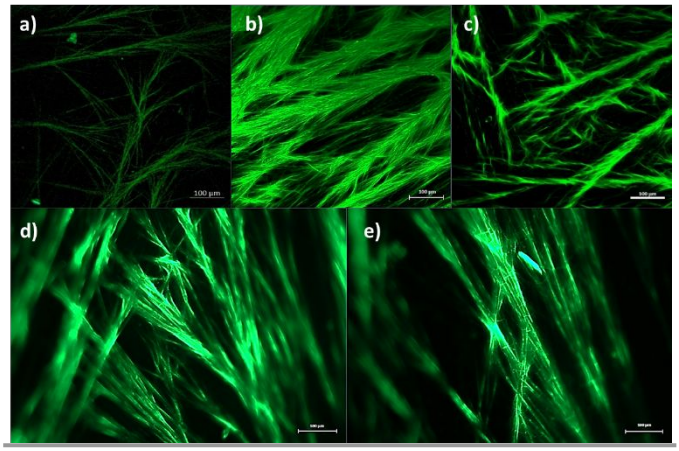

Figure 9. Confocal micrographs of ePLP nanotubes (a), and TC-loaded ePLP nanotubes (b-e).

This is not surprising, because both molecules are rich in motifs with strong H-donors (i.e. in TC –OH and NH_2 groups) and H-acceptors (i.e. in TC, annular and exocyclic carbonyl groups). Consequently, the Raman spectra bands for amide I and II (1605, 1581 cm^{-1}) are shifted by 5 cm^{-1} at least compared to that for non-loaded nanotubes (Supplementary data S9).

TC release from ePLP nanotubes

The quantitative release assays in a physiological-like medium containing ethanol with PLP/TC 1:1, 1:0.5 and 1:0.33 ratios are shown in Figure 10. Of note is that a variety of microenvironments are expected for any given location within the organism (i.e. pH and hydrophilicity/hydrophobicity ratio), and consequently ethanol best represents the myriad of potential physiological conditions within the body. Specifically, this solvent is known to modify the hydrophobicity of the release medium when hydrophobic drugs are delivered, an approach to mimic the hydrophobicity of lipid-and liposome-rich environments.[47] In the present experiment, release profiles always reach an asymptotic value that changes for each ePLP:TC ratio. The values ca. 100%, 60% and 50% are determined after 24 h of exposure for the 1:1, 1:0.5 and 1:0.33 sample ratios, respectively (Figure 10).

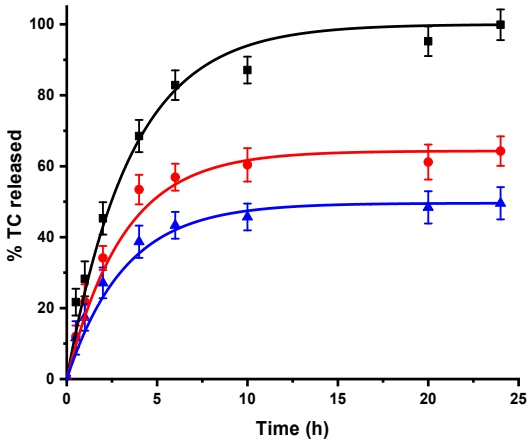

Figure 10. TC release profiles from ePLP/TC 1:1 (black), 1:0.5 (red) and 1:0.33 (blue) in PBS-EtOH. Values correspond to the average while the error bars indicate the standard deviations (i.e. assays were carried out for triplicate).

These results are evident with the analysis of the release kinetics calculated by first-order[48,49] and Higuchi models.[50,51] Drug release occurs in two steps, i.e., a rapid release of drug that should deposit on the surface of ePLP nanotubes, and a slow release that involve the diffusion of drug from nanotube hollows towards the outer medium. In this way, a combined model based on both Higuchi and first-order models describe the 0-60% (first step) and 40-100% (second step) of the release, respectively.[52,53] The kinetic data from the release profiles is shown in Table 2.

Release constants for TC increased gradually with reduction of the drug loading because the diffusion and the establishment of equilibrium conditions is faster. Thus, release of the TC depends on the concentration of ePLP in solution, being the fastest release for 1:0.33 PLP:TC sample ratio with ca. 50% in 24 h (Figure 10). The lowest rates for the other samples might be ascribed to a strong adsorption of the TC to the peptide backbone, thus lowering the diffusion to the medium. After 6 h, the release of the drug for 1:1 and 1:0.5 ePLP:TC ratios becomes even slower than that for 1:0.33 PLP:TC ratio. The occurrence of supramolecular aggregates due to strong TC-PLP electrostatic interactions, and hydrogen bonds, might prevent the complete release of the drug, in agreement to analogous systems previously reported.[54,55]

Table 2. Kinetic parameters for TC release from ePLP/TC nanotubes

ePLP/TC	k_H ($h^{-0.5}$)	r	k_1 (h^{-1})	r
1:1	0.308	0.995	0.197	0.961
1:0.5	0.363	0.982	0.262	0.982
1:0.33	0.380	0.996	0.332	0.971

Conclusions

The self-assembly of the long peptide chains in the ePLP molecule into nanotubes under controlled conditions is demonstrated. Strong analytical evidence supports the physicochemical and morphological characteristics for this ePLP. A remarkable breakthrough in this work is the shift from a poorly ordered and water-soluble macromolecule to a well-defined α-helix nanotube structure with addition of only 1 vol% organic co-solvent. The dielectric and conductivity properties for this macromolecule have been also ascertained. These results add to other reports using PLP produced by SSPS, wherein the solubility and low molecular weights challenge the control of the self-assembly. These features allow for envisaged biomedical applications for the ePLP. Among them, the loading of a TC for delivery studies has been discussed. The distinctive features for the enzyme-mediated PLP compared to other chemical approaches encourages further investigation of this molecule and other enzyme-mediated high molecular weight polypeptides.

Conflicts of interest

There are no conflicts to declare.

Acknowledgements

The authors acknowledge support from PAPIIT (IN200520) and CONACyT for scholarship (A.R.-M. #336576). Luis J. del Valle and Jordi Puiggalí are grateful to a grant (RTI2018-101827-B-100) from MINECO.

References

1 1. J. Wang, K. Liu, R. Xing and X. Yan, *Chemical Society Reviews*, 2016, 45, 5589-5604.
2 2. C. Chen, K. Liu, J. Li and X. Yan, *Advances in colloid and interface science*, 2015, 225, 177-193.
3 3. M. L. Choi and S. Gandhi, *The FEBS journal*, 2018, 285, 3631-3644.
4 4. C. M. Dobson, *Nature*, 2003, 426, 884.
5 5. B. I. Lee, Y. S. Suh, Y. J. Chung, K. Yu and C. B. Park, *Scientific reports*, 2017, 7, 7523.
6 6. Y. Mazor, S. Gilead, I. Benhar and E. Gazit, *Journal of molecular biology*, 2002, 322, 1013-1024.
7 7. S. J. Song, S. Lee, K.-S. Ryu and J. S. Choi, *Bioconjugate chemistry*, 2017, 28, 2266-2276.
8 8. F. Zhang and H. Yan, *Journal*, 2017.
9 9. I. W. Hamley, *Angewandte Chemie International Edition*, 2014, 53, 6866-6881.
10 10. M. Mizrahi, A. Zakrassov, J. Lerner-Yardeni and N. Ashkenasy, *Nanoscale*, 2012, 4, 518-524.
11 11. N. Amdursky, M. Molotskii, E. Gazit and G. Rosenman, *Journal of the American Chemical Society*, 2010, 132, 15632-15636.
12 12. C. Guo, Y. Luo, R. Zhou and G. Wei, *ACS nano*, 2012, 6, 3907-3918.
13 13. N. Habibi, N. Kamaly, A. Memic and H. Shafiee, *Nano Today*, 2016, 11, 41-60.
14 14. S. Kim, J. H. Kim, J. S. Lee and C. B. Park, *Small*, 2015, 11, 3623-3640.
15 15. G. B. Qi, Y. J. Gao, L. Wang and H. Wang, *Advanced Materials*, 2018, 30, 1703444.
16 16. L. Sun, C. Zheng and T. J. Webster, *International journal of nanomedicine*, 2017, 12, 73.
17 17. E. Mayans, G. Ballano, J. Casanovas, L. J. del Valle, M. M. Pérez-Madrigal, F. Estrany, A. I. Jiménez, J. Puiggalí, C. Cativiela and C. Alemán, *Soft matter*, 2016, 12, 5475-5488.
18 18. E. Mayans, G. Ballano, J. Casanovas, A. Díaz, M. M. Pérez-Madrigal, F. Estrany, J. Puiggalí, C. Cativiela and C. Alemán, *Chemistry–A European Journal*, 2015, 21, 16895-16905.
19 19. D. M. Ryan, T. M. Doran, S. B. Anderson and B. L. Nilsson, *Langmuir*, 2011, 27, 4029-4039.
20 20. I. S. Aguirre-Díaz, C. Montiel, I. Bustos-Jaimes, Y. Medina-Gonzalez, A. Tecante and M. Gimeno, *RSC advances*, 2018, 8, 35936-35945.
21 21. K. Tsuchiya and K. Numata, *Polymer Chemistry*, 2020, 11, 560-567.
22 22. K. Tsuchiya and K. Numata, *Macromolecular Bioscience*, 2017, 17.
23 23. C. H. Görbitz, *New Journal of Chemistry*, 2003, 27, 1789-1793.
24 24. F. l. Müller, C. A. Ferreira, D. S. Azambuja, C. Alemán and E. Armelin, *The Journal of Physical Chemistry B*, 2014, 118, 1102-1112.
25 25. C. Cai, L. Wang and J. Lin, *Chemical Communications*, 2011, 47, 11189-11203.
26 26. L. Whitmore and B. A. Wallace, *Biopolymers: Original Research on Biomolecules*, 2008, 89, 392-400.

27 27. N. Amdursky and M. M. Stevens, *ChemPhysChem*, 2015, 16, 2768-2774.
28 28. E. Y. Chi, S. Krishnan, T. W. Randolph and J. F. Carpenter, *Pharmaceutical research*, 2003, 20, 1325-1336.
29 29. C. Zhang, M. Yang and K. Zhao, *Physical Chemistry Chemical Physics*, 2017, 19, 32007-32015.
30 30. C. Diaferia, T. Sibillano, N. Balasco, C. Giannini, V. Roviello, L. Vitagliano, G. Morelli and A. Accardo, *Chemistry–A European Journal*, 2016, 22, 16586-16597.
31 31. M. Reches and E. Gazit, *Science*, 2003, 300, 625-627.
32 32. C. Diaferia, N. Balasco, T. Sibillano, C. Giannini, L. Vitagliano, G. Morelli and A. Accardo, *ChemPhysChem*, 2018, 19, 1635-1642.
33 33. V. L. Sedman, L. Adler-Abramovich, S. Allen, E. Gazit and S. J. Tendler, *Journal of the American Chemical Society*, 2006, 128, 6903-6908.
34 34. J. J. Panda, S. Yandrapu, R. S. Kadam, V. S. Chauhan and U. B. Kompella, *Journal of controlled release: official journal of the Controlled Release Society*, 2013, 172, 1151.
35 35. S. Parween, A. Misra, S. Ramakumar and V. S. Chauhan, *Journal of Materials Chemistry B*, 2014, 2, 3096-3106.
36 36. E. Krieg, M. M. Bastings, P. Besenius and B. Rybtchinski, *Chemical reviews*, 2016, 116, 2414-2477.
37 37. C. H. Görbitz, *Chemistry–A European Journal*, 2001, 7, 5153-5159.
38 38. I. W. Hamley, *Chemical reviews*, 2017, 117, 14015-14041.
39 39. C. G. Pappas, R. Shafi, I. R. Sasselli, H. Siccardi, T. Wang, V. Narang, R. Abzalimov, N. Wijerathne and R. V. Ulijn, *Nature nanotechnology*, 2016, 11, 960.
40 40. W. Ma, A. G. Cheetham and H. Cui, *Nano today*, 2016, 11, 13-30.
41 41. T. Fan, X. Yu, B. Shen and L. Sun, *Journal of Nanomaterials*, 2017, 2017.
42 42. S. Sek, K. Swiatek and A. Misicka, *The Journal of Physical Chemistry B*, 2005, 109, 23121-23124.
43 43. L. Sepunaru, S. Refaely-Abramson, R. Lovrinčić, Y. Gavrilov, P. Agrawal, Y. Levy, L. Kronik, I. Pecht, M. Sheves and D. Cahen, *Journal of the American Chemical Society*, 2015, 137, 9617-9626.
44 44. L. L. Del Mercato, P. P. Pompa, G. Maruccio, A. Della Torre, S. Sabella, A. M. Tamburro, R. Cingolani and R. Rinaldi, *Proceedings of the National Academy of Sciences*, 2007, 104, 18019-18024.
45 45. J. L. Yardeni, M. Amit, G. Ashkenasy and N. Ashkenasy, *Nanoscale*, 2016, 8, 2358-2366.
46 46. K. Tao, P. Makam, R. Aizen and E. Gazit, *Science*, 2017, 358, eaam9756.
47 47. K. Park, D. Choi and J. Hong, *Scientific reports*, 2018, 8, 1-9.
48 48. M. Gibaldi and S. Feldman, *Journal of pharmaceutical sciences*, 1967, 56, 1238-1242.
49 49. H. Liu, K. K. Leonas and Y. Zhao, *Journal of Engineered Fibers and Fabrics*, 2010, 5, 155892501000500402.
50 50. J. G. Wagner, *Journal of pharmaceutical sciences*, 1969, 58, 1253-1257.
51 51. T. Higuchi, *Journal of pharmaceutical sciences*, 1961, 50, 874-875.
52 52. T. Higuchi, *Journal of pharmaceutical sciences*, 1963, 52, 1145-1149.
53 53. R. W. Baker, *Controlled release of biologically active agents*, John Wiley & Sons, 1987.
54 54. A. Puiggalí-Jou, A. Cejudo, L. J. del Valle and C. Alemán, *ACS Applied Bio Materials*, 2018, 1, 1594-1605.
55 55. T. Coviello, F. Alhaique, C. Parisi, P. Matricardi, G. Bocchinfuso and M. Grassi, *Journal of controlled release*, 2005, 102, 643-656.

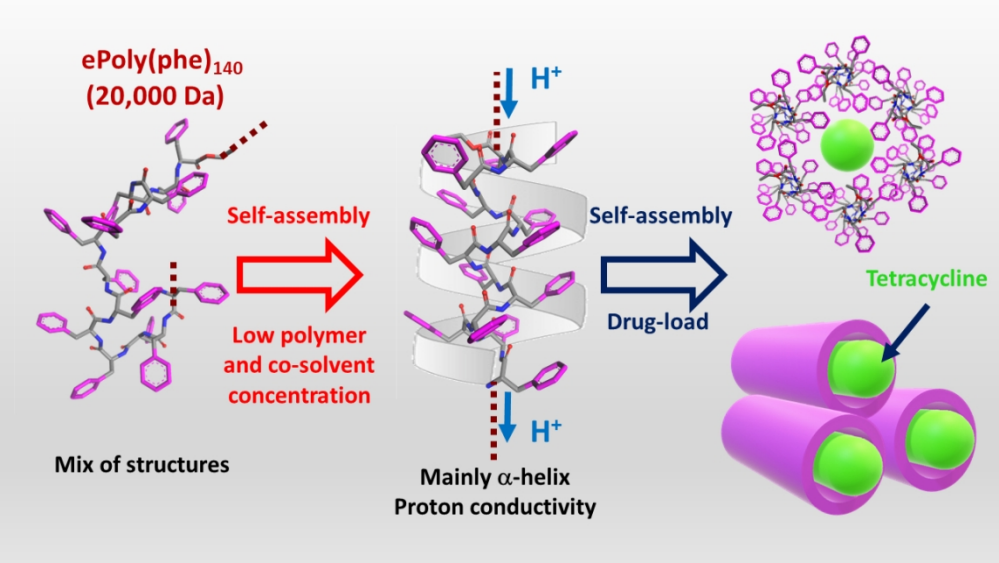
ePoly(phe)140
(20,000 Da)
Self-assembly
Low polymer
and co-solvent
concentration
Mix of structures
H+
H+
Mainly α-helix
Proton conductivity
Self-assembly
Drug-load
Tetracycline

SUPPORTING INFORMATION

Self-assembly of supramolecular chemoenzymatic poly-L-Phenylalanine [poly(Phe)$_{140}$]

Alejandra Romero-Montero,[a] Isabel S. Aguirre-Díaz,[a] Jordi Puiggalí,[b] Luis J. del Valle[b], Miquel Gimeno[a]**

[a] Departamento de Alimentos y Biotecnología, Facultad de Química, Universidad Nacional Autónoma de México, 04510 CDMX, México

[b] Chemical Engineering Department, Escola d'Enginyeria de Barcelona Est-EEBE, c/Eduard Maristany 10-14, Barcelona, Spain

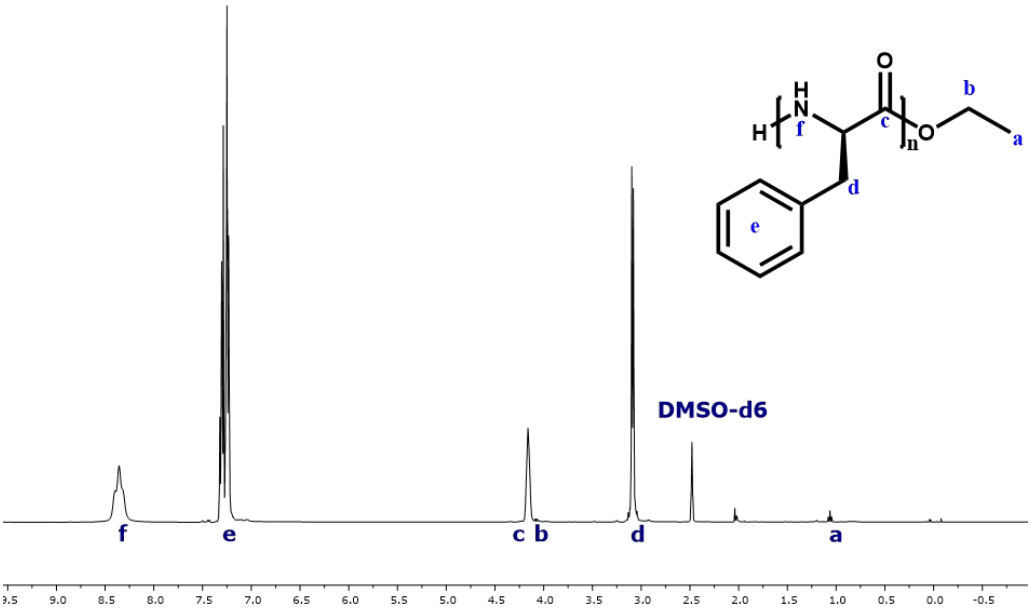

Figure S1. ^{1}H NMR spectra for PLP

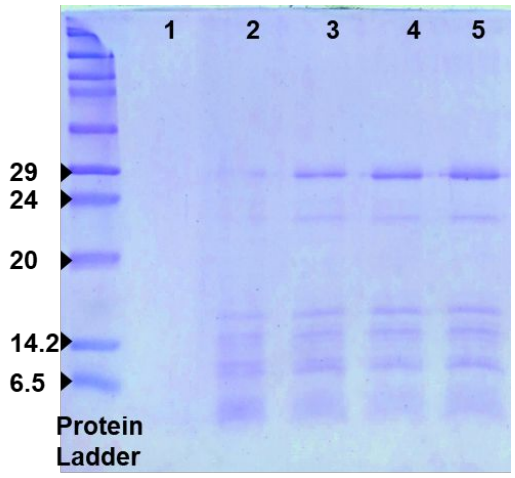

Figure S2. SDS-PAGE of PLP fresh solution from reactor (1), concentrated sample by nano-filtration (2-5).

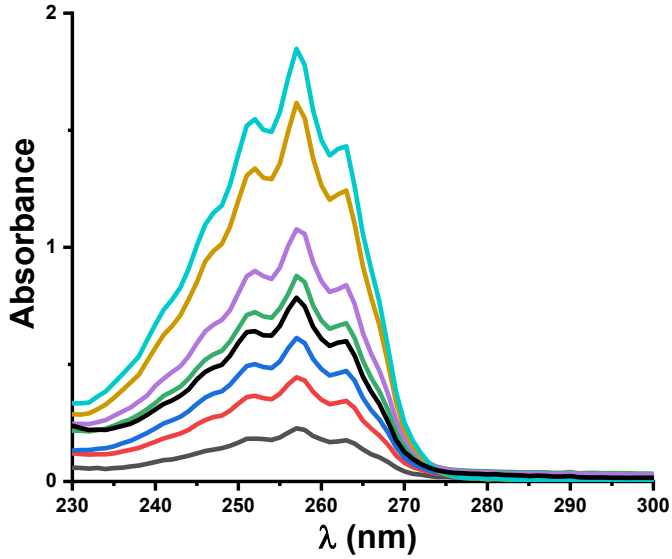

Figure S3-1. UV-vis absorption spectra ($\varepsilon_{257\ nm}$= 2.08 x10^4 L $mol^{-1}cm^{-1}$) with different ePLP concentrations (0.2-1.8 mg/mL).

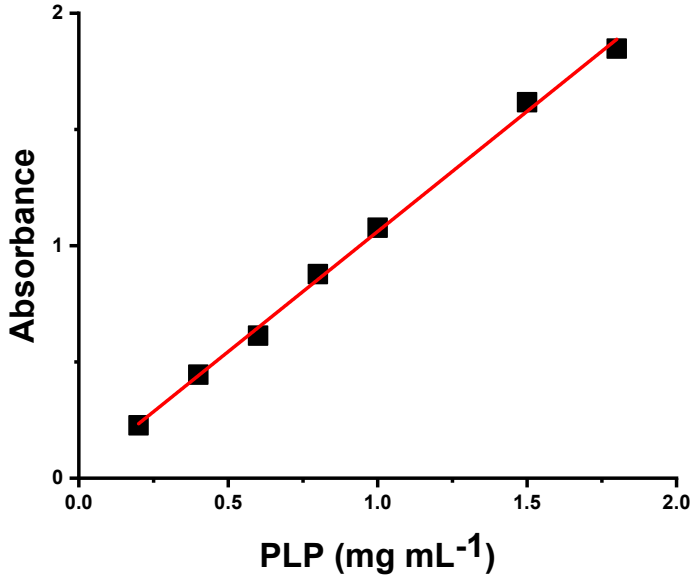

Figure S3-2. Calibration curve for PLP in water by UV-vis spectroscopy.

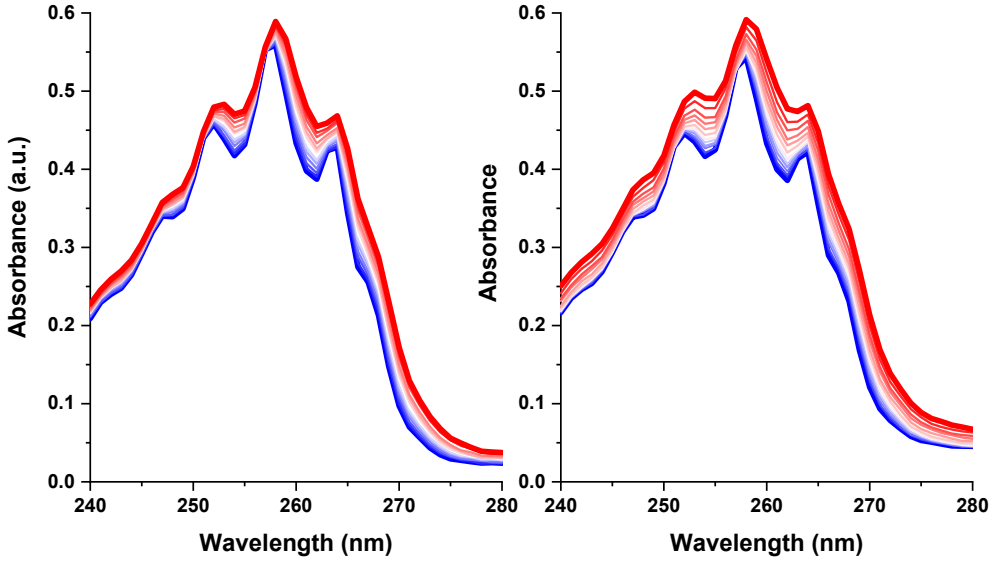

Figure S4. UV spectra upon heating from 25 °C (blue) to 90 °C (red) for water-solubilized (a), and urea-solubilized (b) ePLP.

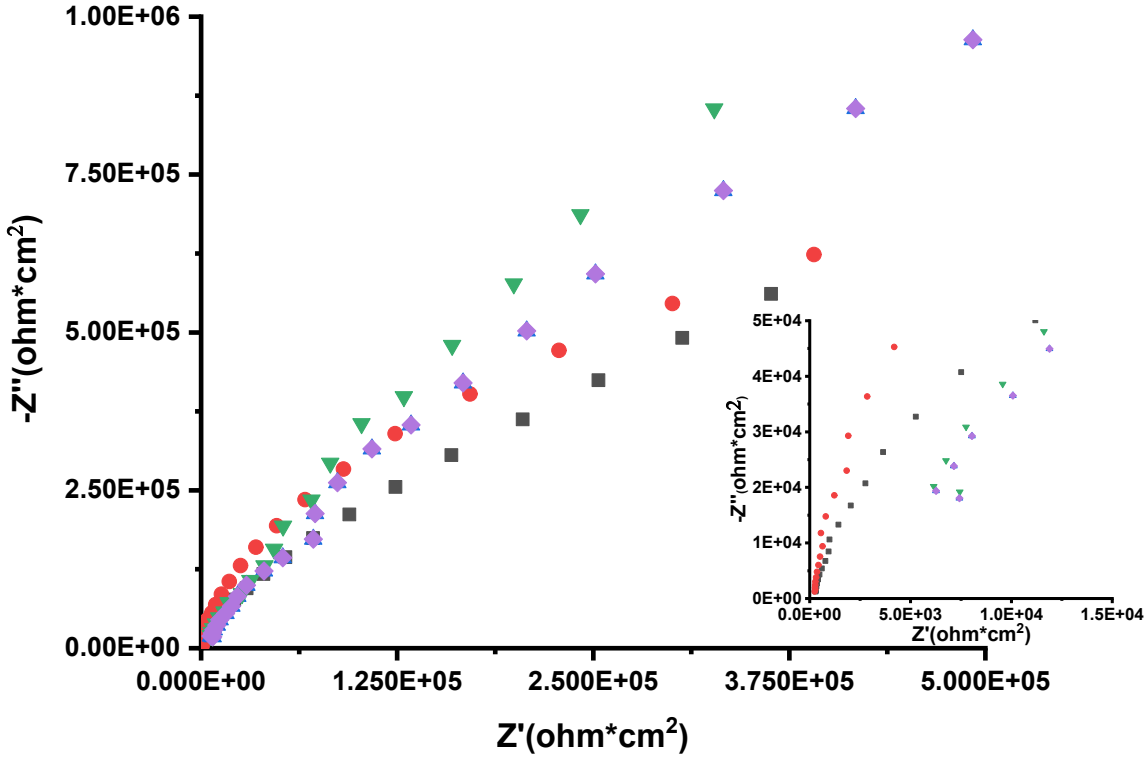

Figure S5. Nyquist plot of ePLP nanotubes (black and red symbols) and ePLP bulk (green and purple symbols). The inset represents a detail of the high- frequency region.

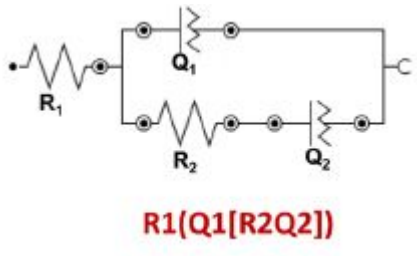

Figure S6. Equivalent electrical circuit

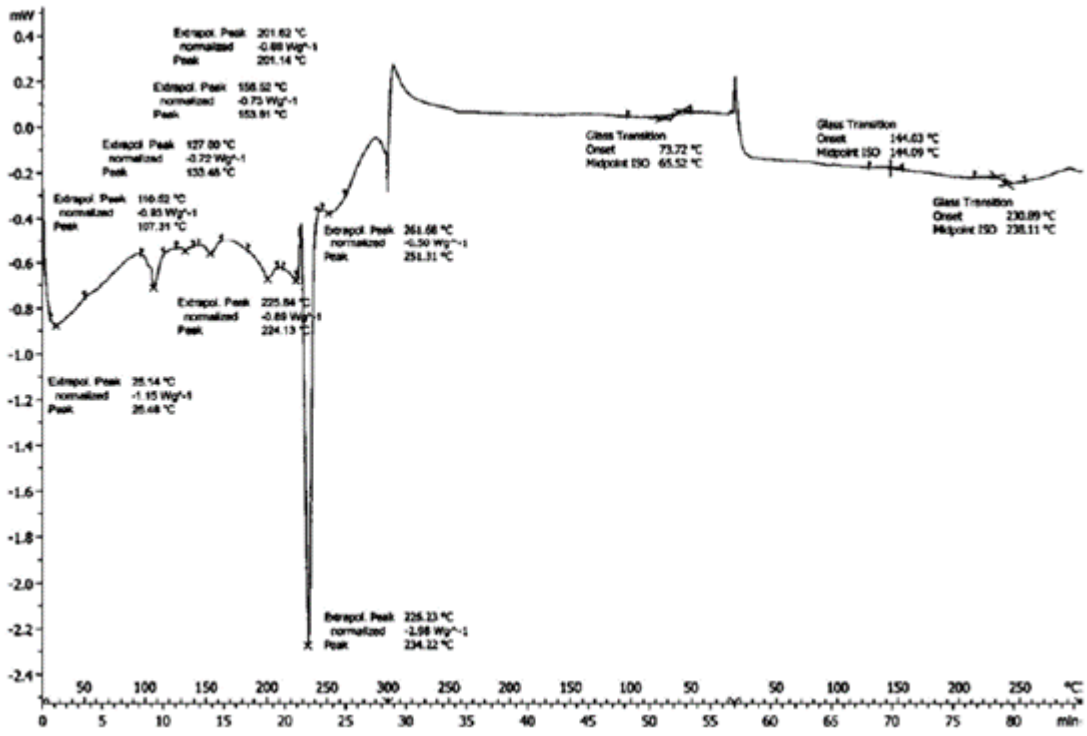

Figure S7. DSC for ePLP.

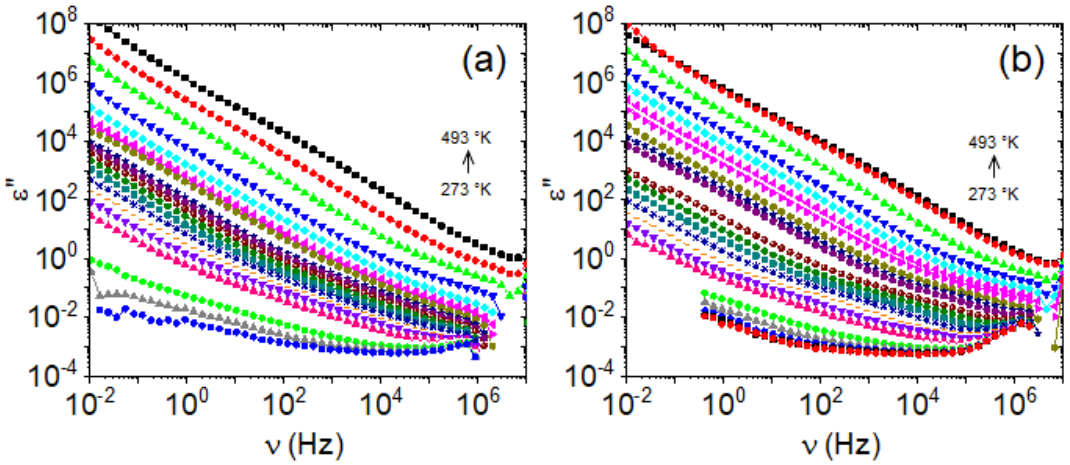

Figure S8. Imaginary part (ε'') of the dielectric constant for disordered (a) and nanotubes ePLP (b).

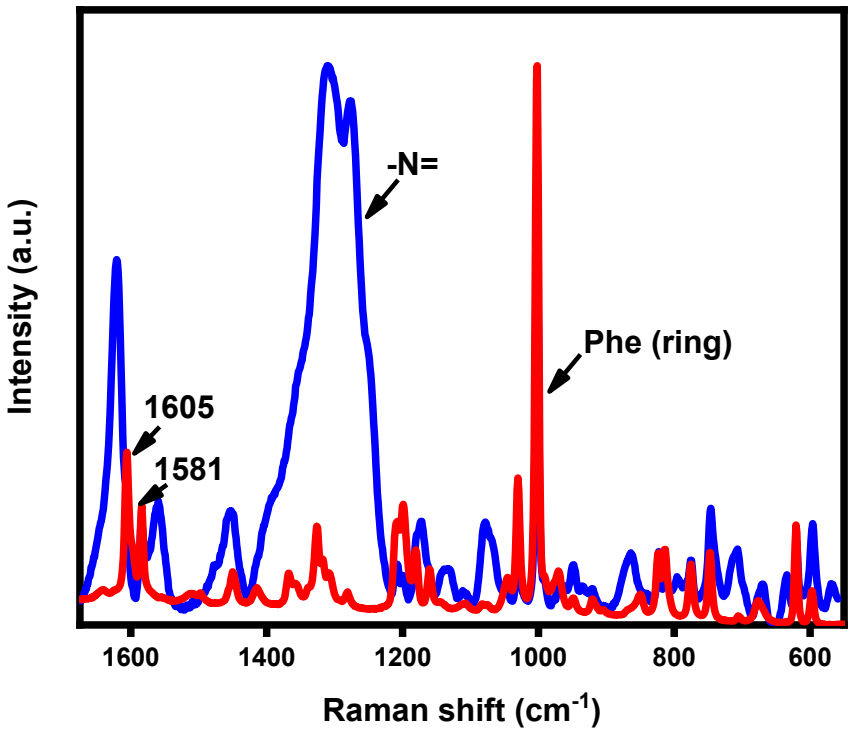

Figure S9. Raman spectra for PLP nanotubes (red); and TC-loaded PLP nanotubes (blue).